journal

J. Am. Ceram. Soc., 94 [1] 237–244 (2011)
DOI: 10.1111/j.1551-2916.2010.04021.x

Nanostructured Alumina from Freeze-Dried Precursors

Regina Villanueva, Andrés Gómez, Pedro Burguete, Eduardo Martínez, Aurelio Beltrán, and Fernando Sapiña†

Institut de Ciència dels Materials, Parc Cientific, Universitat de València, PO Box 22085, 46071 Valéncia, Spain

Mónica Vicent and Enrique Sánchez

Instituto de Tecnología Cerámica—Asociación de Investigación de las Industrias Cerámicas, Universitat Jaume I, 12006 Castellón, Spain

Nanocrystalline alumina has been obtained on the 100 g scale by thermal decomposition of precursors resulting from the freeze-drying of aqueous solutions of different aluminum-containing products, namely aluminum acetate and aluminum L-lactate. Samples prepared at different temperatures (from 873 to 1573 K in steps of 100 K) were characterized by X-ray powder diffraction (XRD), scanning electron microscopy (SEM) and transmission electron microscopy (TEM), and surface area measurements. In the acetate case, the transformation sequence involves the formation of θ-Al_2O_3 as an intermediate phase between γ-Al_2O_3 and α-Al_2O_3, whereas this θ phase is not observed in the lactate case. TEM and SEM images show the nanoparticulate character of the aluminas obtained at relatively low temperatures, with typical particle size in the 5–10 nm range. Progressive grain growth occurs as temperature increases. Otherwise, the precursor characteristics have a clear influence on the microstructure of the resulting aluminas, as reflected also by the measured BET surface area values. Whereas long aluminum acetate fibers results in open arrays of low aggregated alumina particles, large aluminum lactate sheets lead to comparatively compact alumina microstructures. Nanostructured alumina obtained from the lactate precursor has been reconstituted in a granulated powder with sufficient consistence and flowability to allow it to be thermal sprayed and deposited on a stainless steel substrate. XRD data show that γ-Al_2O_3 is the major phase in the coating, which includes also α-Al_2O_3 particles. SEM results offer evidences on the nanostructured character of the coating.

I. Introduction

There is an increasing awareness of the potential of nanostructured coatings, both for replacing present coatings, due to their superior properties in comparison with their conventional (microstructured) counterparts, and for generating new applications.[1,2] Studies have centered on ceramic–metal composites (cermets of the WC–Co type) and ceramic oxides.[3–7] The reason for this choice is based on the particular characteristics of ceramic materials, such as high hardness and high thermal and corrosion resistance, which provide many advantages compared with polymers and metals when it comes to use as coatings, especially in applications in which wear, temperature, and corrosion resistance are simultaneously required.

Although several methods have already been used to date to prepare nanostructured coatings (sputtering, sol–gel, etc.), the process that is most likely to find industrial implementation in the short term is thermal spraying and, in particular, plasma spraying, owing to its great versatility.[8] In plasma thermal spraying (atmospheric plasma spraying (APS) being the most widespread method), the nanostructured starting powder is heated in a high-temperature gas stream to a semifused state, while concurrently being accelerated toward the substrate to be coated.[9–14] When this material impacts the substrate, small lens-like deposits form (known as "splats"), approximately 20 μm in diameter and 5 μm thick, from the semifused state. These splats solidify quickly at cooling rates of approximately 100 K/s. Coatings with thickness up to 200–300 μm can be produced by increasing the number of spray gun passes. Because this is a rapid process, in which the residence times during which the materials are exposed to high temperatures are extremely short, it might favor holding the nanostructure of the starting powder in the coating. In fact, progress of feedstock particles melting (a process that has been thoroughly studied) depends on both plasma spraying conditions and the very nature of the feedstock.[15,16] Thus, the maintenance of the starting powder nanostructure should be practically guaranteed in nonmelted zones. We will return on this point later on.

Under this approach, the seemingly obvious requirement for obtaining nanostructured coatings is to have the adequate nanostructured starting powder at our disposal. Nanostructured materials are ultrafine-grained solids with a high proportion of atoms at grain boundaries. The key factor for industrial exploitation of nanostructured materials lies in the development of cost-effective, large-scale manufacturing processes.[17,18] At present, more than two dozen different processes for their preparation have been described. However, most of these methods are expensive, require sophisticated equipment, and yield relatively low production rates. Therefore, they have high production costs and are conceived for obtaining high-value-added materials, with typical applications in the fields of electronics and photonics. In other cases, difficulties may appear owing to operation details. Indeed, a problem frequently associated with sol–gel-related methods lies in the stoichiometric control and the cation distribution in multicomponent systems.

In this context, powder processing methods for the preparation of submicrometer and nanostructured powders in a controlled form, with a wide range of compositions, sizes, and morphologies, need to be improved. The freeze-drying method was first successfully applied by E. W. Flosdorf in 1935 in the instant coffee industry. Nowadays, this method is applied in the production of numerous advanced materials.[19–32] The method consists of (a) fast freezing of a sprayed solution, (b) vacuum drying by sublimation of the solvent, and (c) decomposition of the resulting precursor to give rise to oxides, nitrides, or carbides by heat treatment in a controlled atmosphere. In comparison with other chemical methods, one of the advantages of this

J. Smialek—contributing editor

Manuscript No. 27691. Received March 15, 2010; approved June 28, 2010.
This study was supported by the Spanish Ministry of Science and Technology and EU FEDER Program (MAT2006-12945-C0-01, MAT2006-12945-C0-03, MAT2009-14144-C03-01, and MAT2009-14144-C03-03).
†Author to whom correspondence should be addressed. e-mail: fernando.sapina@uv.es

technique is its capacity to prepare polycrystalline powders with controlled characteristics. The commercial applications (electronics, pharmacy, catalysis, pigments, etc.) are determined by the specific properties of the resulting materials. As far as other competing synthesis processes are concerned, the disadvantages of the sol–gel method (difficult control of the stoichiometry and cation distribution in multicomponent systems) have been noted above. In the spray-drying method, on the other hand, the equipment has a high volume and a low production rate.

Alumina and mixtures of alumina and titania are used as coatings that withstand severe high temperature, friction, or corrosion environments.[33–35] The present paper reports on how the use of freeze-dried precursors allows the preparation of nanostructured alumina powders at the 100 g scale. The nanostructured alumina was reconstituted in a granulated powder with sufficient consistency and flowability to allow it to be sprayed and deposited on stainless steel substrates.

II. Experimental Procedure

(1) Synthesis

(A) Materials: The materials used as reagents in this study were aluminum hydroxide, $Al(OH)_3$ (Kemira Ibérica, Barcelona, Spain, 100%), aluminum L-lactate, $Al(CH_3CHOHCOO)_3$ (Aldrich, St. Louis, MO, 97.0%), cerium (III) acetate hydrate, $Ce(CH_3COO)_3 \cdot 1.5H_2O$ (Aldrich, 99.9% pure), glacial acetic acid (Panreac, Castellar del Vallès, Spain 99.5%), and acetic anhydride (Panreac 98%).

(B) Preparation of Precursors: Aluminum hydroxide was transformed in a soluble acetate complex by refluxing for 24 h in a suspension containing $Al(OH)_3$ (0.7 mol) in a 1:1 (v:v) mixture of glacial acetic acid and acetic anhydride (50 mL). Then, the suspension was filtered and the resulting solid was washed with acetone. The precursor solution was prepared by refluxing for 3 h in a suspension of the acetate complex (0.024 mol) in water (200 mL), which resulted in a clean solution whose concentration in Al^{3+} was 0.12*M*.

Aluminum L-lactate precursor solution (0.60*M* in Al^{3+}) was directly prepared by dissolving the salt (0.15 mol) in water (250 mL) under continuous stirring at room temperature. We also prepared a second precursor solution in which a small amount of cerium was present (Ce^{3+}:Al^{3+} = 1:100 mol; $[Al^{3+}] = 0.60M$). Addition of cerium has the purpose of avoiding the carbon deposition observed on the products resulting from thermal decomposition of the cerium-free precursor at low temperatures. Cerium was handled as cerium (III) acetate, and was dissolved in the aluminum L-lactate solution. On the other hand, for considering possible effects on the microstructure of the final alumina associated with the concentration of the precursor solution, we also prepared analogous solutions whose concentration in Al^{3+} was 0.12*M*. In order to improve efficiency for further treatments, the precursor solutions must be as concentrated as solubility allow.

Droplets of these solutions were flash frozen by spraying on liquid nitrogen and, then, freeze-dried at a pressure of 10^{-4} atm in a Telstar Cryodos freeze-drier (Terrasa, Spain). In this way, dried solid precursors were obtained as amorphous (X-ray diffraction (XRD)) loose powders. The thermal evolution of the precursors was monitored by thermogravimetric experiments (TGA–DTA) under oxygen atmosphere (heating rate 5 K/min, flow rate 50 cm^3/min), using a Setaram Setsys 16/18 system (Caluire, France).

(C) Synthesis of Nanostructured Alumina: Nanostructured alumina samples were synthesized by thermal decomposition of the amorphous precursor solids. A sample of the selected precursor was placed into an alumina boat and introduced in the furnace. Several runs under different experimental conditions were performed in order to determine its influence on the structure and microstructure of the samples. The precursor powder was heated at 5 K/min to a final temperature T_f (T_f = 573–1573 K, in steps of 100 K) that was held for a period of time t_{hold} of 6 h under flowing oxygen. The solid was then cooled by leaving the sample inside the furnace (slow cooling, ca. 2 K/min). All products were stored in a desiccator over $CaCl_2$.

(D) Preparation of an Alumina Coating from Nanostructured Powder

(a) Feed Powders: In most thermal spray methods, coatings are obtained from feedstock in powder form. As a result, in order to obtain nanostructured coatings by these techniques, it is convenient to use nanoparticles as raw material. However, nanoparticles cannot be sprayed directly owing to their low mass: they must be agglomerated to form micrometric particles. This process, which is critical for the success of the method, is known as reconstitution process. In fact, agglomerate size and density are critical for coating quality. The powder must be dense enough and have an appropriate particle-size distribution. Fine and porous powders cannot be fed into the center of the plasma flame. Indeed, they will float on the flame surface or will be evaporated by superheating before spattering on the substrate, which results in poor deposition efficiency and poor coating bond strength.

Nanostructured alumina agglomerates with good cohesion and sufficient mechanical strength were prepared by forcing the granular association of precursor particles. With this aim, an aqueous solution (10 wt%) of polyvinyl alcohol (PVA, Mowiol 4/88 from Clariant, Mutlenz, Switzerland) was used. A sample of the nanostructured alumina powder was deposited on a tray and sprayed with the PVA solution. It was then transferred to a granulating drum, which was rotated at 200 rpm for 10 min. The amount of PVA added was ca. 1.0 wt% (referred to powder sample). The resulting granulated powder was screened between 40 and 100 μm. Finally, in order to enhance powder flowability, fumed silica (Aerosil 200 from Evonik, Essen, Germany) was added to the granulated powder, and this mixture was again rotated in the drum for 10 min. The amount of fumed silica added was ca. 0.6 wt% (referred to powder sample).

(b) Coating Processing by APS: APS is one of the most important and versatile techniques currently used by various sectors of industry for the deposition of wear-resistant ceramic coatings. During the process, the feedstock is injected in powder form inside the flame at very high temperature (6000–12 000 K). The powder is heated and accelerated until impact on the substrate surface, where it cools rapidly, and forms the coating.

In this study, coatings were obtained by APS (Sulzer-Metco F4 MB plasma gun, Winterthur, Switzerland), mounted on an industrial robot (IRB1400 from ABB, Zurich, Switzerland). Before spraying, the substrate was blasted with corundum grit and cleaned with ethanol to remove any dust or grease residue from the surface. The main spraying parameters were as follows: Ar flow rate, 35 slpm (standard liter per minute); H_2 flow rate, 12 slpm; arc intensity, 600 A; spraying velocity 1000 mm/s; and spraying distance 120 mm.

(3) Characterization

(A) Elemental Analysis: Metal ratios in the cerium-containing samples were determined by energy-dispersive X-ray analysis (EDAX) on a scanning electron microscope (Hitachi S-4100, (Tokyo, Japan) BSE Autrata detector, EMIP 3.0 Software, and a RONTEC microanalysis system, Berlin, Germany). Operating voltage was 20 kV, ;and the energy range of the analysis was 0–20 keV. EDAX showed that the freeze-dried precursors were homogeneous at micrometer scale.

(B) XRD: XRD patterns were obtained from a diffractometer using Cu$K\alpha$ radiation (Seifert XRD 3003 TT, Ahrensburg, Germany). Samples were dusted through a sieve on the holder surface. Routine patterns were collected with a scanning step of 0.08° at 2θ over the angular range 2θ 10°–70° with a collection time of 5 s per step. All graphical representations relating to XRD patterns were performed using adequate software (DRX-Win Program).[36] This technique was also used to characterize the as-sprayed coating.

(C) Microstructural Characterization: The morphology of the freeze-dried precursors, the resulting oxides, and the

as-sprayed coating were observed using a scanning electron microscope–field emission (Hitachi 4100FE) operating at an accelerating voltage of 30 kV, and using also a transmission electron microscope (JEOL JEM 1010, Tokyo, Japan) operating at an accelerating voltage of 100 kV. All the scanning electron microscopic (SEM) preparations were covered with a thin film of gold for better image definition.

(D) Surface Areas: The BET surface areas of the products were determined by nitrogen adsorption at 77 K, assuming a cross-sectional area of 0.162 nm^2 for the nitrogen molecule (Micromeritics ASAP 2000, Norcross, GA). Before adsorption measurements, the samples were outgassed in vacuum at 423 K for 18 h.

III. Results

The thermal evolution of the precursors was monitored by TGA and XRD. Figure 1 shows the TGA curves corresponding to the thermal evolution under oxygen atmosphere (heating rate 5 K/min, flow rate 50 cm^3/min) of the different freeze-dried powder precursors. In all cases, the onset of the thermal decomposition of the organic component of the precursor complexes occurs at ca. 475 K, and decomposition is complete at 675–700 K. Before this process (i.e., from room temperature until ca. 475 K), a relatively small (3–12 wt%) and continuous weight loss is observed for all samples, which could be associated with evolution of water molecules retained in the precursors. After water removal, decomposition of the precursors occurs in at least two-step superimposed processes.

Figure 2 shows the XRD patterns of the products resulting from thermal treatment of the precursors at temperatures ranging from 1073 to 1473 K. The thermal treatments were performed under dynamic oxygen atmosphere for 6 h. In the case of the Al acetate samples, the presence of aluminum oxyhydroxide was observed at 573 and 673 K. By rising the treatment temperatures, it appeared firstly (773 K) an amorphous product, whereas transition aluminas were detected from 873 to 1273 K. Concerning these transition aluminas, γ-Al_2O_3 is the only crystalline product between 873 and 1073 K, while θ-Al_2O_3 is observed at 1173 and 1273 K. Although θ-Al_2O_3 remains as the major phase at 1373 K, we can now also observe weak peaks attributable to α-Al_2O_3. The α-Al_2O_3 phase becomes the major one at 1473 K, but the presence of θ-Al_2O_3 results in some weak peaks. Finally, at 1573 K, α-Al_2O_3 is the only detectable phase. Thus, the transformation sequence in the thermal decomposition of the acetate precursor can be written as follows:

Otherwise, dealing with the aluminum lactate samples, the final products from thermal treatments ranging from 573 to 973 K were amorphous. Crystallization of the γ-Al_2O_3 phase can be observed at 1073 K. Formation of α-Al_2O_3 is not detected (as minor phase) until 1273 K. Finally, α-Al_2O_3 appears as the only crystalline phase at 1373 K and higher temperatures. In the case of Al–Ce lactate samples, the transformation sequence is similar to that described for the lactate precursor exempt from Ce. However, the α-Al_2O_3 appears at higher temperatures. In fact, both α-Al_2O_3 and transition γ-Al_2O_3 phase peaks are observed at 1373 K. It is interesting to note that the CeO_2 peaks are not detected at relatively low temperatures (i.e., in the presence of γ-Al_2O_3). In fact, the CeO_2 peaks are not observed before the formation of some α-Al_2O_3 (1373 K). These two facts suggest that (a) γ-Al_2O_3 is able to form a solid solution that incorporates Ce(IV) ions, (b) the presence of dissolved Ce(IV) ions stabilizes γ-Al_2O_3 with respect to α-Al_2O_3, and (c) the solubility limit of Ce(IV) in α-Al_2O_3 is very low. Thus, the transformation sequences in the thermal decomposition of the lactate precursors are as follows:

$$\text{Aluminum lactate precursor} \rightarrow \text{amorphous product} \rightarrow \gamma\text{-}Al_2O_3 \rightarrow \alpha\text{-}Al_2O_3$$

$$\text{Al}-\text{Ce lactate precursor} \rightarrow \text{amorphous product} \rightarrow \gamma\text{-}(Al, Ce)_2O_3 \rightarrow \alpha\text{-}Al_2O_3 + CeO_2$$

The poor crystallinity of the low-temperature polymorphs (γ and θ), as well as the influence on peak width of the disorder in the cation positions, prevents a clear picture of the temperature evolution of the crystallite size of these phases from being obtained. However, information was obtained on the α-Al_2O_3 crystallite size. This size was calculated from XRD patterns by a standard Scherrer analysis of the half-width of the XRD peaks. LaB_6 from NIST (SRM660a) (Gaithersburg, MD) was used as standard to calibrate the intrinsic width associated with the equipment.[37] Crystallite sizes range, in all cases, from 70 to 200 nm, depending on the temperature and precursor. Thus, even at 1573 K, the α-Al_2O_3 crystallites are very small.

Figures 3–5 show characteristic transmission electron microscopic and SEM images corresponding to some representative alumina samples. In the case of the Al acetate precursor, the freeze-dried powder is made up of fibers, several hundred nanometers long, with a diameter of about 5–10 nm. The external appearance of these fibers remains practically unchanged during the thermal decomposition process, as can be clearly observed in the micrograph of the sample prepared at 1073 K (Fig. 3(a)). However, these fibers are now constituted by aggregates of nanometric particles with a typical size of 5–10 nm. At higher temperatures, a continuous small increase in particle size is observed, together with a progressive collapse of the fibrillar microstructure. Between 1373 and 1573 K (Fig. 3(b)), the collapse of the fibrillar array produces an open structure.

$$\text{Aluminum acetate precursor} \rightarrow AlO(OH) \rightarrow \text{amorphous product} \rightarrow \gamma\text{-}Al_2O_3 \rightarrow \theta\text{-}Al_2O_3 \rightarrow \alpha\text{-}Al_2O_3$$

In the case of the aluminum lactate precursor, the evolution of the microstructure displays some differences. Indeed, the freeze-dried precursor consists of sheets with typical dimensions of 4000 nm × 4000 nm × 500 nm. Again, the external appearance of the precursor particles remains practically unchanged during relatively low temperature treatments (1073 K), as can be clearly observed in the micrograph shown in Fig. 4(a). A higher magnification image reveals that the product sheets consist of aggregates of nanoparticles with a typical size of 5–10 nm (Fig. 4(b)). At higher temperatures, a certain increase in particle

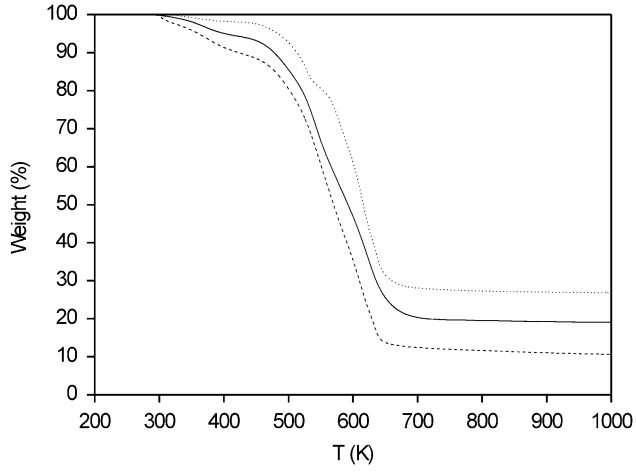

Fig. 1. Characteristic TGA curves corresponding to Al acetate (dotted line), aluminum lactate (solid line), and Al–Ce lactate (dashed line) freeze-dried precursors.

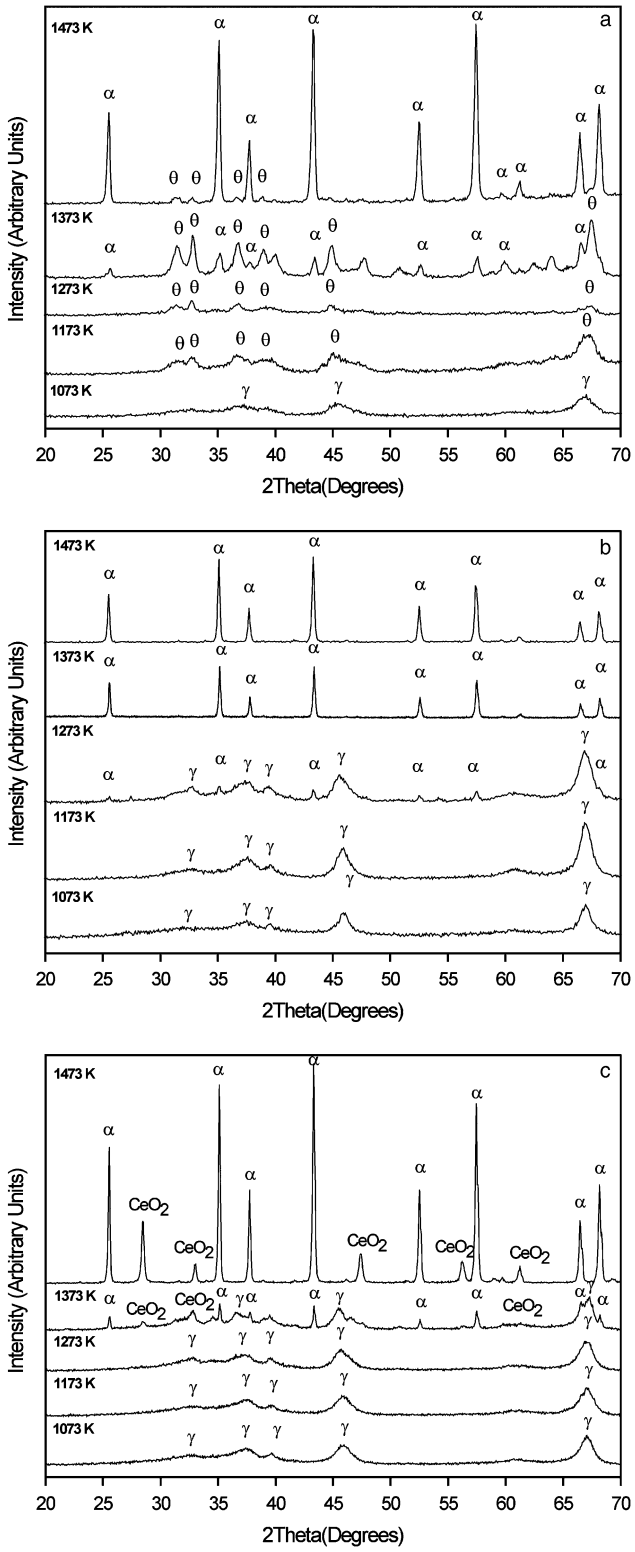

Fig. 2. X-ray diffraction patterns of materials prepared by thermal decomposition in oxygen of (a) Al acetate freeze-dried precursor, (b) aluminum lactate freeze-dried precursor, and (c) Al–Ce lactate freeze-dried precursor. The temperatures of the thermal treatment are 1073–1473 K, in 100 K intervals, from bottom to top, in all cases.

size is observed (Fig. 4(c)). At 1573 K, strong grain growth and sintering is observed (Fig. 4(d)).

Insofar as differences in precursor concentration salts (0.12*M* for Al acetate and 0.60*M* for aluminum lactate) could have some influence on the microstructural characteristics of the final products (because of effects due to the agglomeration degree after freeze-drying), we carried out comparative experiments starting from an aluminum L-lactate precursor solution 0.12*M* in Al^{3+}. It must be stressed that neither XRD patterns nor SEM micrographs corresponding to analogous products in these series (0.60 or 0.12*M* aluminum lactate) reveal any noticeable difference. So, the observed differences in the behavior of samples coming from aluminum acetate and aluminum L-lactate precursors should be related to the proper precursor nature, and not associated with concentration effects.

In the Al–Ce lactate case, the evolution of the microstructure is very similar to that of the aluminum lactate precursor: the large sheets of the original precursor are observed until 1373 K (Fig. 5(c)), and consist of nanoparticle aggregates that grow slowly between 1073 and 1373 K (Figs. 5(a) and (b)). At 1573 K, strong grain growth and sintering is observed (Fig. 5(d)). However, there is a significant difference with respect to the aluminum lactate case: the presence on the surface of sintered grains of small particles with a typical size of about 80 nm. According to XRD data, the presence of these small particles can be attributed to the segregation of CeO_2 during the γ-Al_2O_3 to α-Al_2O_3 transformation.

These differences in the final microstructures, either open or more compact depending on the precursor, are clearly reflected in the evolution of the BET surface area of the samples (Fig. 6). At a given temperature, the BET surface area of alumina samples coming from the acetate precursor are significantly larger than those corresponding to lactate-derived samples.

Figure 7 shows the XRD of the coating prepared by using as feedstock nanostructured alumina obtained from the aluminum lactate precursor at 1073 K. As observed, γ-Al_2O_3 is the major phase in the coating but the presence of α-Al_2O_3 is evident. According to previous results in the literature, this is a usual situation: independent of the type of alumina used to apply the coating, the presence of mixtures of γ-Al_2O_3 and α-Al_2O_3 is always observed, the relative contents of both phases being mainly related to the sprayed aggregate size.[38,39]

Figure 8 shows micrographs of the coating corresponding to both the outer layer (Figs. 8(a) and (b)) and an inner surface as resulting from a transversal fracture (Figs. 8(c) and (d)). As can be observed (Fig. 8(a)), the porous as-sprayed surface exhibits an irregular topography. One can clearly appreciate the final image of the sprayed droplets (splats) together with zones in which comparatively small pseudofaceted particles prevail. Very likely, the as-observed splats became deformed and partially disaggregated by hitting the substrate. When these splats are examined at higher magnification (Fig. 8(b)), their surface appears as consisting of a highly compact array of nanoparticles. Otherwise, the surface generated after fracture shows the same microstructural features (splats and particle zones) than the outer layer (Fig. 8(c)). Figure 8(d) shows a representative image, at high magnification, focused on a zone exempt from splats. As observed, the surface of the pseudofaceted particles is also composed of nanoparticles. By comparison with the splats case, these nanoparticles are higher and adopt a less compact disposition.

IV. Discussion

It is well known that alumina crystallizes in many polymorphs.[40–47] All these polymorphs can be classified into two groups, based on the arrangement of oxygen anions. There are structures based on a cubic compact packing (fcc), such as the γ, η, θ, or δ forms, or on a hexagonal compact packing (hcp), such as the α, κ, and χ forms. The differences between the polymorphs belonging to the same group are related to the arrangement of the cations in the holes of the compact packing of oxide anions. It is, thus, very difficult to differentiate among the polymorphs in each group. The different polymorphs are obtained by thermal decomposition of a variety of precursors. Depending on the precursor (e.g., polymorphs of aluminum oxyhydroxide or hydroxide), different Al_2O_3 structures are formed, which follow diverse sequences of phase transformations with

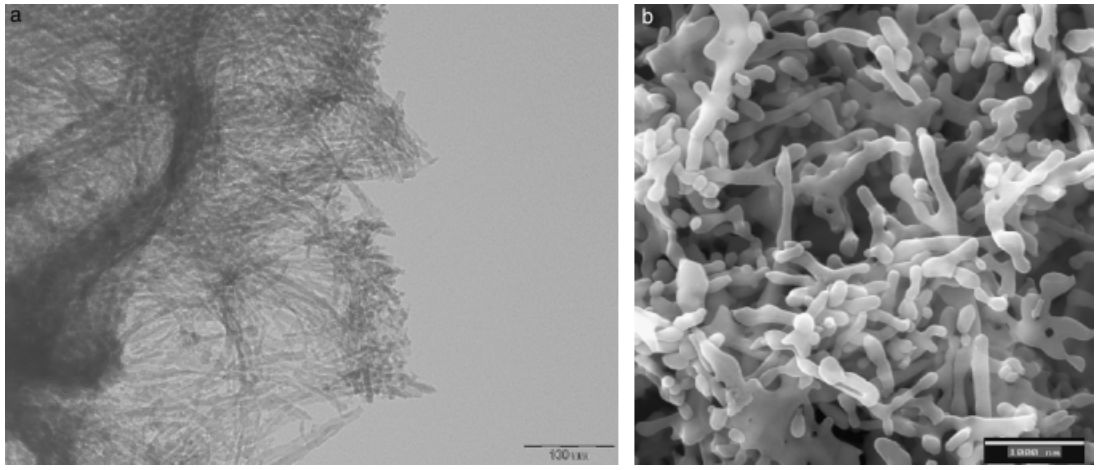

Fig. 3. Transmission electron microscopic (TEM) and scanning electron microscopic (SEM) images showing the microstructure of the materials obtained from Al acetate freeze-dried precursors: (a) 1073 K (TEM); (b) 1573 K (SEM). Scale bars correspond to 100 and 1000 nm, respectively.

increasing temperature. In all cases, the α form is the thermodinamically stable at high temperatures under normal conditions. The detailed sequences and stability ranges have been attributed to many factors, such as crystallinity degree, presence of impurities, thermal history, among others.

Without prejudice to the above, there is abundant information in the literature supporting the idea that the alumina particle size has a great influence on the crystalline form adopted: nanoparticulate alumina crystallizes in the γ form and microparticulate alumina in the α form.[48] This is not an unique situation: nanoparticulate TiO_2 and ZrO_2 crystallize in anatase and tetragonal forms, respectively, and microparticulate TiO_2 and ZrO_2 in rutile and monoclinic forms, respectively.[49,50] Most researchers indicate that the microparticulate samples of these oxides adopt the thermodynamically stable structural variety, whereas those shown by nanoparticulate samples are

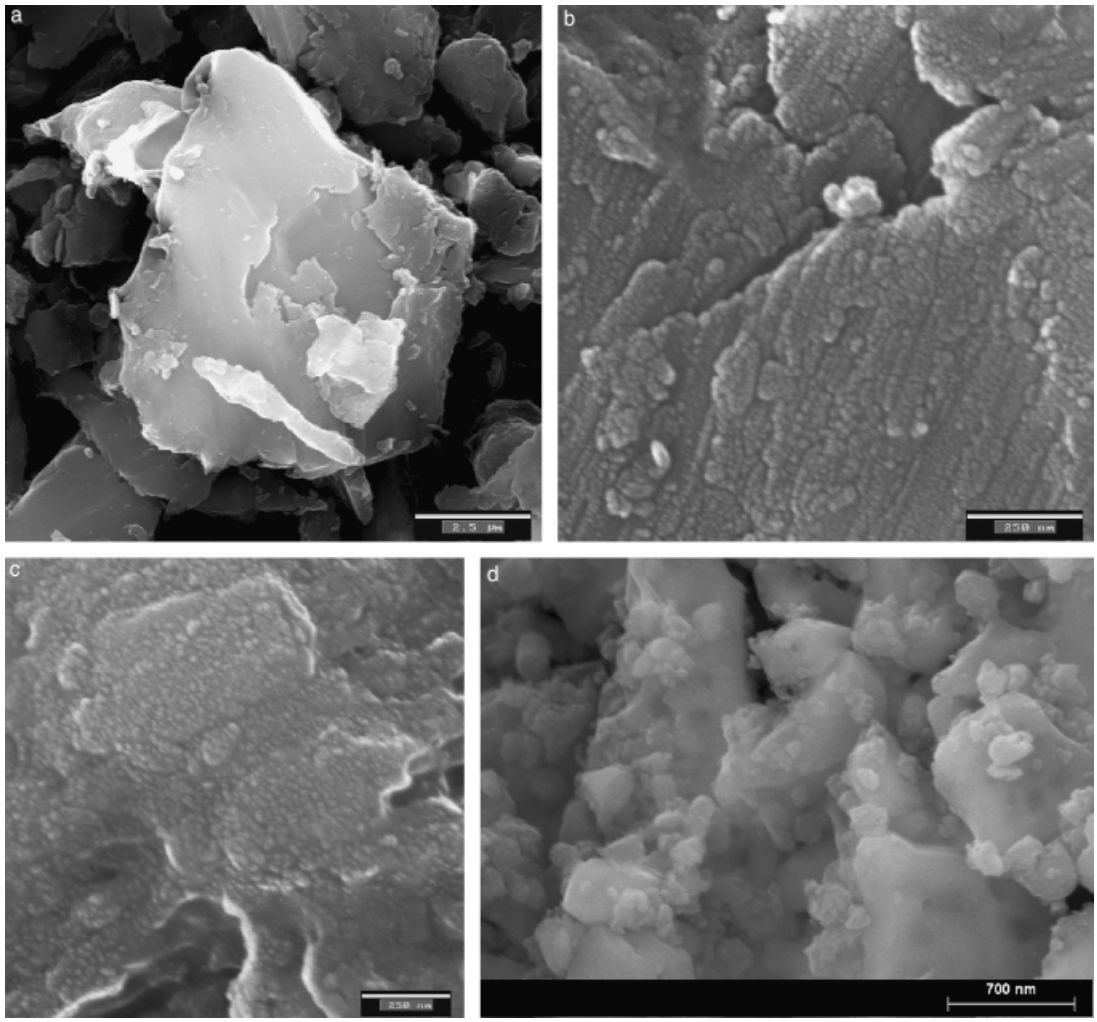

Fig. 4. Scanning electron microscopic images showing the microstructure of the materials obtained from aluminum lactate freeze-dried precursors: (a and b) 1073 K, (c) 1273 K, and (d) 1573 K. Scale bars correspond to 2.5 μm, 250, 250, and 700 nm, respectively.

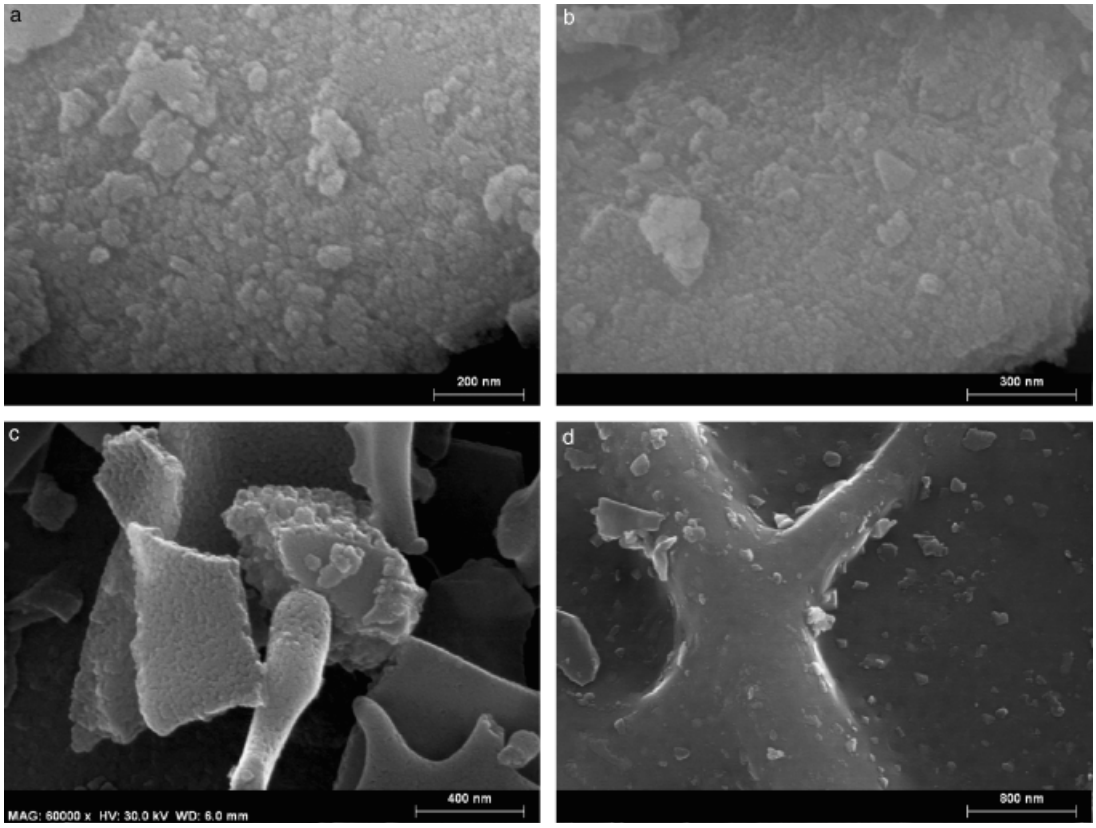

Fig. 5. Scanning electron microscopic images showing the microstructure of the materials obtained from Al–Ce lactate freeze-dried precursors: (a) 1073 K, (b and c) 1373 K, and (d) 1573 K. Scale bars correspond to 200, 300, 400, and 800 nm, respectively.

metastable.[49] However, in 1993, molecular dynamic simulation of different γ-Al_2O_3 and α-Al_2O_3 surfaces indicated that the surface energies of α-Al_2O_3 were significantly greater than those of γ-Al_2O_3.[51] These data suggested that γ-Al_2O_3 becomes the energetically stable polymorph of nanoparticulate alumina, as it was claimed by Navrotsky and colleagues in 1997.[52] After few months, the group of Navrotsky reported experimental results showing that the surface energy of α-Al_2O_3 is actually significantly greater than that of γ-Al_2O_3 (2.64 vs 1.67 J/m^2, respectively). As they concluded, this implies, in practice, that surface energy differences thermodynamically stabilize nanoparticulate γ-Al_2O_3 over nanoparticulate α-Al_2O_3.[53] Since then, this group has applied the same methodology, using high-temperature solution calorimetry data coupled with other techniques, to demonstrate that similar surface energy differences also explain the TiO_2, ZrO_2, and anhydrous and hydrated ferric oxides cases.[54–56]

Because the samples in this study are aggregated, we cannot obtain information on the surface area at which stability crossover occurs. Note, furthermore, that the aggregation state of the studied alumina samples depends on the precursor: it is low in the acetate case, and very high in the lactate case. Indeed, aluminas obtained from acetate, lactate, and Ce lactate precursors have BET surface areas of 156, 21, and 41 m^2/g, respectively, at 1173 K. These differences in the aggregation state of the samples are in turn due to differences in the microstructure of the original precursor: the fibrillar microstructure of the acetate precursors produces an open and poorly aggregated microstructure in the resulting aluminas, whereas the lamellar microstructure of lactate precursors produces a compactly aggregated microstruc-

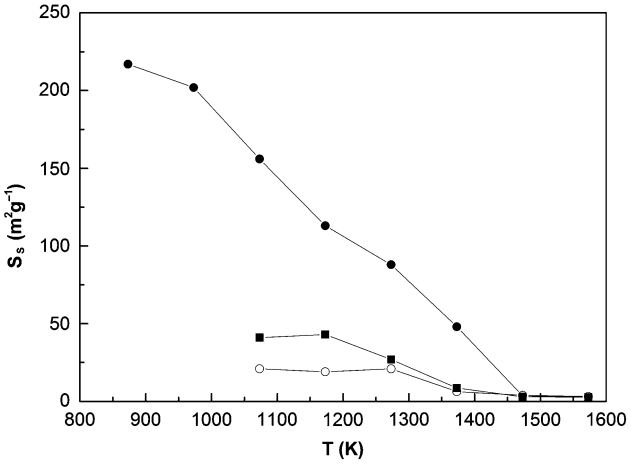

Fig. 6. Evolution of the BET area with the preparation temperature of the samples. Closed circles, acetate precursor samples; open circles, lactate precursor samples; and closed square, Ce lactate precursor samples.

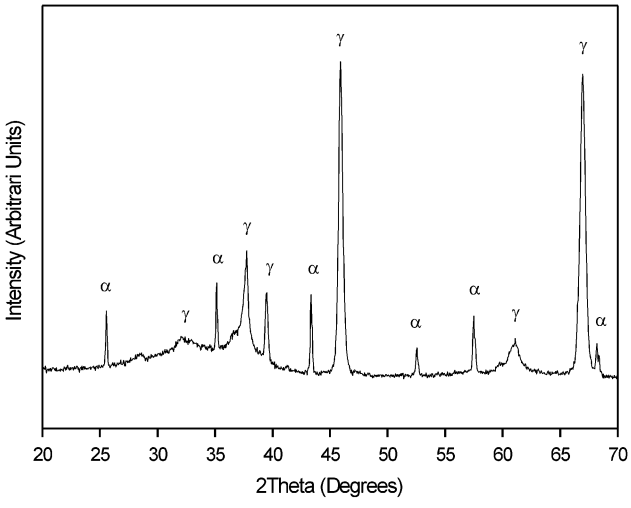

Fig. 7. X-ray diffraction pattern of the plasma-sprayed coating.

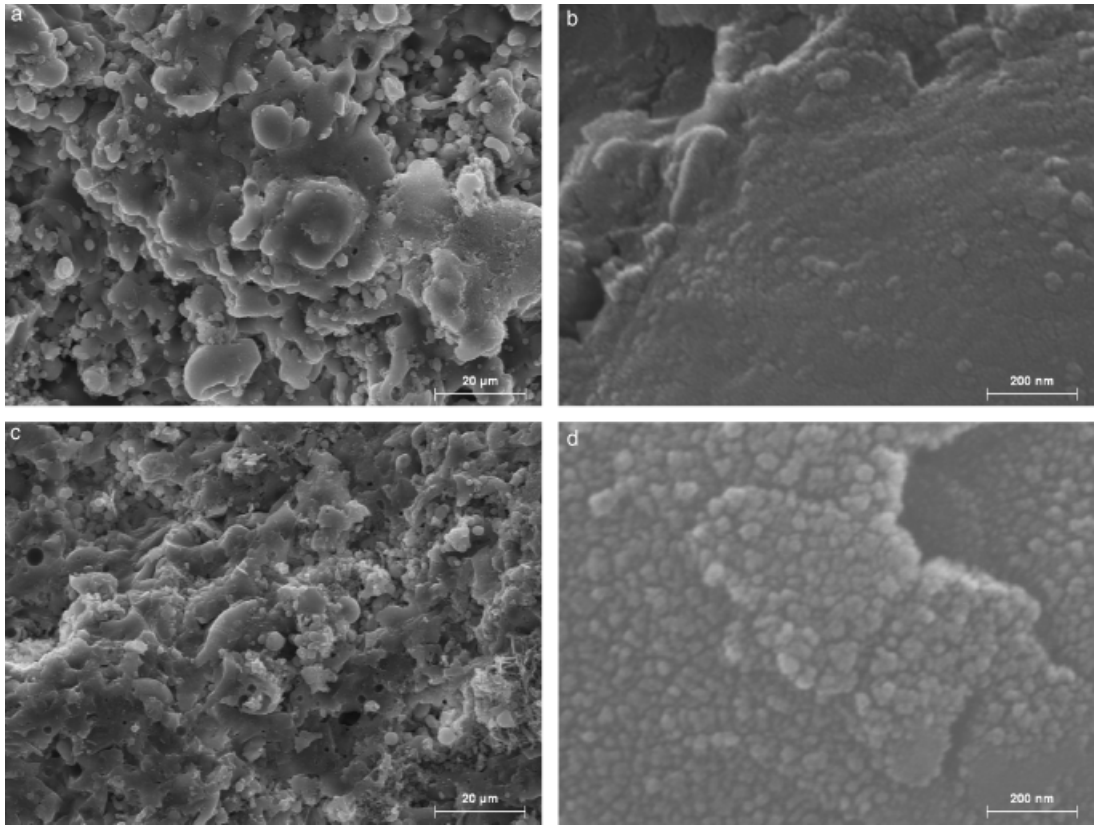

Fig. 8. Scanning electron microscopic images showing the microstructure of the plasma-sprayed coating: (a and b) surface, and (c and d) fracture views. Scale bars correspond to 20 μm, 200 nm, 20 μm, and 200 nm, respectively.

ture. Owing to aggregation, it is clear that not all the surface is accessible for BET measurement. Thus, interfacial energies must contribute significantly to the total surface energy in the lactate-derived samples, whereas their contribution must be relatively low in the acetate-derived samples. Even more, the transformation sequence in the case of the acetate precursor includes the presence of θ-Al_2O_3, whereas this phase is not observed in the transformation sequences of the lactate precursors. This strongly suggests that the presence of θ-Al_2O_3 can be attributed to a stabilization of this phase due to an energy crossover favored at low aggregation degrees, but suppressed at high aggregation degrees.

Finally, some remarks need to be made concerning the coating characteristics. As noted above, although our powder feedstock was conformed by agglomeration of nanoparticulate γ-Al_2O_3, the XRD data show that the coating is built up from both γ-Al_2O_3 and α-Al_2O_3. This is a systematic result concerning nanostructured alumina thermally sprayed coatings: independent of the structural variety used as feedstock, the resulting coating consists of mixtures of γ-Al_2O_3 and α-Al_2O_3.[38,39] In the thermal plasma treatment, the nanoparticle agglomerates are subjected to very high temperatures. Depending on both the agglomerate features and plasma parameters, partial or total melting of the agglomerates occurs. Because of the high temperature conditions, the possible nonfused (solid) regions in the generated droplets should mainly consist of particles of the stable α-Al_2O_3. The short residence time does not make probable significant further particle growth by sintering. On hitting the substrate, quenching of the melt, at rates exceeding 100 K/s, leads to the formation of a great number of crystallization nuclei, which have low chance for growing. Thus, solidification (crystallization) of liquid droplets at considerable undercooling should result in the formation of γ-Al_2O_3 rather than α-Al_2O_3, according to the stability crossover characterized by Navrotsky *et al.*[53] The observed two-scale structure of the thermally sprayed coating (splats from molten regions of the agglomerates cementing retained solid particles) is what could be expected on a thermodynamic basis. In practice, this would make unnecessary kinetic *ad hoc* arguments to explain the presence of γ-Al_2O_3 when α-Al_2O_3 is used as feedstock.[57] In any case, the key role played by the feedstock powder microstructure features in determining the coating microstructure and thermomechanical properties make necessary further studies in order to adjust spray parameters for improving coating performances.[16]

V. Conclusion

In summary, alumina can be successfully prepared as nanoparticles on the 100 g scale by thermal decomposition at relatively low temperatures of precursors obtained by freeze-drying solutions of aluminum acetate or aluminum L-lactate. The formation process shows that θ-Al_2O_3 is produced as an intermediate phase in the acetate case, whereas this phase is not observed in the lactate case. The authors attribute this fact to the different aggregation state of the alumina particles, which depends on the microstructure of the corresponding precursor. A Ce-containing lactate precursor was also prepared in order to avoid the deposition of residual carbon in the course of the precursor decomposition at low temperature. Whereas Ce seems to be dissolved in γ-Al_2O_3, cerium oxide is clearly observed once α-Al_2O_3 has formed. Finally, nanostructured alumina obtained from lactate precursor calcined at 1073 K has been reconstituted into a granulated powder with sufficient consistency and flowability to allow it to be sprayed and deposited on stainless steel substrates. Thermal sprayed coating partly retains the nanostructured character of the alumina powder.

Acknowledgments

The SCSIE of the Universitat de València is gratefully thanked for the use of the X-ray diffraction, electron microscopy, and analytical facilities.

References

[1]A. D. H. Cavaleiro and T. Jeff, *Nanostructured Coatings*. Springer, New York, 2006.

[2]S. C. Tjong and H. Chen, "Nanocrystalline Materials and Coatings," *Mater. Sci. Eng. R*, **44**, 1–88 (2004).
[3]J. H. He and J. M. Schoenung, "Nanostructured Coating," *Mater. Sci. Eng. A*, **336**, 274–319 (2002).
[4]M. D. Salvador, J. J. Candel, V. Bonache, F. Segovia, V. Amigo, E. Sanchez, and V. Cantavella, "Comportamiento a desgaste de recubrimientos de WC proyectados por plasma a partir de polvos micro y nanoestructurados," *Revista de Metalurgia*, **44**, 222–32 (2008).
[5]Y. Wang, W. Tian, and Y. Yang, "Thermal Shock Behavior of Nanostructured and Conventional Al_2O_3/13 wt% TiO_2 Coatings Fabricated by Plasma Spraying," *Surf. Coat. Technol.*, **201**, 7746–54 (2007).
[6]J. H. He and J. M. Schoenung, "A Review on Nanostructured WC–Co Coatings," *Surf. Coat. Technol.*, **157**, 72–9 (2002).
[7]E. H. Jordan, M. Gell, Y. H. Sohn, D. Goberman, L. Shaw, S. Jiang, M. Wang, T. D. Xiao, Y. Wang, and P. Strutt, "Fabrication and Evaluation of Plasma Sprayed Nanostructured Alumina–Titania Coatings with Superior Properties," *Mater. Sci. Eng. A*, **301**, 80–9 (2001).
[8]X. L. Jiang, C. B. Liu, and F. Lin, "Overview on the Development of Nanostructured Thermal Barrier Coatings," *J. Mater. Sci. Technol.*, **23**, 449–56 (2007).
[9]F. L. Trifa, G. Montavon, and C. Coddet, "On the Relationships Between the Geometric Processing Parameters of APS and the Al_2O_3–TiO_2 Deposit Shapes," *Surf. Coat. Technol.*, **195**, 54–69 (2005).
[10]S. Guessasma and C. Coddet, "Microstructure of APS Alumina–Titania Coatings Analysed Using Artificial Neural Network," *Acta Mater.*, **52** [17] 5157–64 (2004).
[11]S. Guessasma and M. Bounazef, "Experimental Design to Study the Effect of APS Process Parameters on Friction Behavior of Alumina–Titania Coatings," *Adv. Eng. Mater.*, **6**, 907–10 (2004).
[12]H. Choi and C. Lee, "Responses of an Atmospheric Plasma Sprayed (APS) Alumina–Titania Coating to Scratch Wear," *J. Ceram. Process. Res.*, **5**, 214–22 (2004).
[13]M. Bounazef, S. Guessasma, G. Montavon, and C. Coddet, "Effect of APS Process Parameters on Wear Behaviour of Alumina–Titania Coatings," *Mater. Lett.*, **58**, 2451–5 (2004).
[14]H. Choi, C. Lee, and H. Kim, "Effects of the Plasma Gas Composition on the Coating Formation and Coating Properties of the APS Al_2O_3–TiO_2 Coating," *J. Ceram. Process.*, **3**, 210–5 (2002).
[15]R. S. Lima and B. R. Marple, "Thermal Spray Coatings Engineered from Nanostructured Ceramic Agglomerated Powders for Structural, Thermal Barrier and Biomedical Applications: A Review," *J. Therm. Spray Technol.*, **16**, 40–62 (2007).
[16]P. Fauchais, G. Montavon, and G. Bertrand, "From Powders to Thermally Sprayed Coatings," *J. Therm. Spray Technol.*, **19**, 56–80 (2010).
[17]C. C. Koch, *Nanostructured Materials: Processing, Properties and Applications*, 2nd edition, Taylor & Francis, Norwich, 2006.
[18]C. N. R. Rao, A. Müller, and A. K. Cheetham, "Nanomaterials: An Introduction"; pp. 1–11 in *The Chemistry of Nanomaterials: Synthesis, Properties and Applications*, Edited by C. N. R. Rao. A. Müller, and A. K. Cheetham. Wiley-VCH, Weinheim, 2004.
[19]G. Chen and W. Wang, "Role of Freeze Drying in Nanotechnology," *Drying Technol.*, **25**, 29–35 (2007).
[20]C. Tallon, R. Moreno, and M. I. Nieto, "Synthesis of γ-Al_2O_3 Nanopowders by Freeze-Drying," *Mater. Res. Bull.*, **41**, 1520–9 (2006).
[21]W. M. Zeng, A. A. Rabelo, and R. Tomasi, "Synthesis of α-Al_2O_3 Nanopowder by Sol–Freeze Drying Method," *Adv. Powder Technol.*, **189**, 16–20 (2001).
[22]N. Nikolic, L. Mancic, Z. Marinkovic, O. Milosevic, and M. M. Ristic, "Preparation of Fine Oxide Ceramic Powders by Freeze-Drying," *Ann. Chim. Sci. Mat.*, **26**, 35–41 (2001).
[23]O. A. Shlyakhtin, Y.-J. Oh, and Y. D. Tretyakov, "Preparation of Dense $La_{0.7}Ca_{0.3}MnO_3$ Ceramics from Freeze-Dried Precursors," *J. Eur. Ceram. Soc.*, **20**, 2047–54 (2000).
[24]Y. D. Tretyakov, N. N. Oleynikov, and O. A. Shlyakhtin, *Cryochemical Technology of Advanced Materials*. Chapman & Hall Ltd., London, 1997.
[25]Y. Ng-Lee, F. Sapiña, E. Martinez-Tamayo, J. V. Folgado, R. Ibañez, F. Lloret, and A. Segura, "Low-Temperature Synthesis, Structure and Magnetoresistance of Submicrometric $La_{1-x}K_xMnO_{3+\delta}$ Perovskites," *J. Mater. Chem.*, **7**, 1905–9 (1997).
[26]T. Boix, Z. El Fadli, F. Sapiña, E. Martinez, A. Beltran, J. Vergara, R. J. Ortega, and K. V. Rao, "Electronic Properties of Mixed Valence Manganates: The Role of the Cationic Vacancies," *Chem. Mater.*, **10**, 1569–75 (1998).
[27]Z. El Fadli, E. Coret, F. Sapiña, E. Martinez, A. Beltran, and D. Beltran, "Low Temperature Synthesis, Structure and Magnetic Properties of $La_{0.85}(Na_{1-x}K_x)_{0.15}MnO_3$ Perovskites: The Role of A Cation Size Disparity in the Electronic Properties of Mixed-Valence Manganates," *J. Mater. Chem.*, **9**, 1793–9 (1999).
[28]A. El-Himri, M. Cairols, S. Alconchel, F. Sapiña, R. Ibañez, D. Beltran, and A. Beltran, "Freeze-Dried Precursor-Based Synthesis of New Vanadium–Molybdenum Oxynitrides," *J. Mater. Chem.*, **9**, 3167–71 (1999).
[29]A. El-Himri, F. Sapiña, R. Ibañez, and A. Beltran, "Synthesis of New Vanadium–Chromium and Chromium–Molybdenum Oxynitrides by Direct Ammonolysis of Freeze-Dried Precursors," *J. Mater. Chem.*, **10**, 2537–41 (2000).
[30]A. El-Himri, F. Sapiña, R. Ibañez, and A. Beltran, "Pd_2Mo_3N: A New Molybdenum Bimetallic Interstitial Nitride," *J. Mater. Chem.*, **11**, 2311–4 (2001).
[31]R. X. Valenzuela, G. Bueno, A. Solbes, F. Sapiña, E. Martínez, and V. Cortés-Corberán, "Nanostructured Ceria-Based Catalysts for Oxydehydrogenation of Ethane with CO_2," *Top Catal*, **15**, 181–8 (2001).
[32]D. Vie, N. Valero, E. Martinez, F. Sapiña, J. V. Folgado, and A. Beltran, "A New Approach to the Synthesis of Intermetallic Compounds: Mild Synthesis of Submicrometric Co_xM_y (M = Mo, W; x:y = 3:1 and 7:6) Particles by Direct Reduction of Freeze-Dried Precursors," *J. Mater. Chem.*, **12**, 1017–21 (2002).
[33]J. Zang, J. He, Y. Dong, X. Li, and D. Yan, "Microstructure Characteristics of Al_2O_3–13 wt.% TiO_2 Coating Plasma Spray Deposited with Nanocrystalline Powders," *J. Mater. Process. Technol.*, **197** [1–3] 31–5 (2008).
[34]J. Zang, J. He, Y. Dong, X. Li, and D. Yan, "Microstructure and Properties of $A1_2O_3$–13 % TiO_2 Coatings Sprayed Using Nanostructured Powders," *Rare Met.*, **26**, 391–7 (2007).
[35]M. Gell, E. H. Jordan, Y. H. Sohn, D. Goberman, L. Shaw, and T. D. Xiao, "Development and Implementation of Plasma Sprayed Nanostructured Ceramic Coatings," *Surf. Coat. Technol.*, **146–147**, 48–54 (2001).
[36]V. Primo-Martín, "DRXWin & CreaFit 2.0: Graphical and Analytical Tools for Powder XRD Patterns," *Powder Diffrac.* **14**, 70–3 (1999).
[37]A. K. West, *Solid State Chemistry and Its Applications*. John Wiley and Sons, Chichester, UK, 1984.
[38]R. McPherson, "On the Formation of Thermally Sprayed Alumina Coatings," *J. Mater. Sci.*, **15**, 3141–9 (1980).
[39]G. N. Heintze and S. Uematsu, "Preparation and Structures of Plasma-Sprayed γ- and α-Al_2O_3 Coatings," *Surf. Coat. Technol.*, **50**, 213–22 (1992).
[40]I. Levin and D. J. Brandon, "Metastable Alumina Polymorphs: Crystal Structures and Transition Sequences," *J. Am. Ceram. Soc.*, **81**, 1995–2012 (1998).
[41]C. Wolverton and K. C. Hass, "Phase Stability and Structure of Spinel-Based Transition Aluminas," *Phys. Rev. B*, **63** [024102] 1–16 (2000).
[42]S.-H. Cai, N. Rashkeev, S. T. Pantelides, and K. Sohlberg, "Phase Transformation Mechanism between γ- and θ-Alumina," *Phys. Rev. B*, **67** [224104] 1–10 (2003).
[43]G. Paglia, C. E. Buckley, A. L. Rohl, B. A. Hunter, R. D. Hart, J. V. Hanna, and L. T. Byrne, "Tetragonal Structure Model for Boehmite-Derived γ-Alumina," *Phys. Rev. B*, **68** [144110] 1–11 (2003).
[44]G. Paglia, C. E. Buckley, A. L. Rohl, R. D. Hart, K. Winter, A. J. Studer, B. A. Hunter, and J. V. Hanna, "Boehmite Derived γ-Alumina System. 1. Structural Evolution with Temperature, with the Identification and Structural Determination of a New Transition Phase, γ'-Alumina," *Chem. Mater.*, **16**, 220–36 (2004).
[45]G. Paglia, C. E. Buckley, T. J. Udovic, A. L. Rohl, F. Jones, C. F. Maitland, and J. Connolly, "Boehmite-Derived γ-Alumina System. 2. Consideration of Hydrogen and Surface Effects," *Chem. Mater.*, **16**, 1914–23 (2004).
[46]G. Paglia, A. L. Rohl, C. E. Buckley, and J. D. Gale, "Determination of the Structure of γ-Alumina from Interatomic Potential and First-Principles Calculations: The Requirement of Significant Numbers of Nonspinel Positions to Achieve an Accurate Structural Model," *Phys. Rev. B*, **71** [224115] 1–16 (2005).
[47]S. V. Tsybulya and G. N. Kryukova, "Nanocrystalline Transition Aluminas: Nanostructure and Features of X-Ray Powder Diffraction Patterns of Low-Temperature Al_2O_3 Polymorphs," *Phys. Rev. B*, **77** [024112] 1–13 (2008).
[48]P. Ayyub, V. R. Palkar, S. Chattopadhyay, and M. Multani, "Effect of Crystal Size Reduction on Lattice Symmetry and Cooperative Properties," *Phys. Rev. B*, **51**, 6135–8 (1995).
[49]R. C. Garvie, "The Occurrence of Metastable Tetragonal Zirconia as a Crystallite Size Effect," *J. Phys. Chem.*, **69**, 1238–43 (1965).
[50]A. A. Gribb and J. F. Banfield, "Particle Size Effects on Transformation Kinetics and Phase Stability in Nanocrystalline TiO_2," *Am. Mineral.*, **82**, 717–28 (1997).
[51]S. Blonski and S. H. Garofaini, "Molecular Dynamics Simulations of α-Alumina and γ-Alumina Surfaces," *Surf. Sci.*, **295**, 263–74 (1993).
[52]J. M. McHale, A. Navrotsky, and A. J. Perrotta, "Effects of Increased Surface Area and Chemisorbed H_2O on the Relative Stability of Nanocrystalline γ-Al_2O_3 and α-Al_2O_3," *J. Phys. Chem. B*, **101**, 603–13 (1997).
[53]J. M. McHale, A. Auroux, A. J. Perrotta, and A. Navrotsky, "Surface Energies and Thermodynamic Phase Stability in Nanocrystalline Aluminas," *Science*, **277**, 788–91 (1997).
[54]M. R. Ranade, A. Navrotsky, H. Z. Zhang, J. F. Banfield, S. H. Elder, A. Zaban, P. H. Borse, S. K. Kulkarni, G. S. Doran, and H. J. Whitfield, "Energetics of Nanocrystalline TiO_2," *Proc Natl Acad Sci*, **99** [Suppl. 2] 6476–81 (2002).
[55]M. W. Pitcher, S. V. Ushakov, A. Navrotsky, B. F. Woodfield, G. Li, J. Boerio-Goates, and B. M. Tissue, "Energy Crossovers in Nanocrystalline Zirconia," *J. Am. Ceram. Soc.*, **88**, 160–7 (2005).
[56]A. Navrotsky, L. Mazeina, and J. Majzlan, "Size-Driven Structural and Thermodynamic Complexity in Iron Oxides," *Science*, **319**, 1635–8 (2008).
[57]D. Zois, A. Lekatou, M. Vardavoulias, I. Panagiotopoulos, and A. Vazdirvanidis, "A Comparative Microstructural Investigation of Nanostructured and Conventional Al_2O_3 Coatings Deposited by Plasma spraying," *J. Therm. Spray Technol.*, **17**, 887–94 (2008). □